CFTR therapeutics normalize cerebral perfusion deficits in mouse models of heart failure and subarachnoid hemorrhage

Darcy Lidington, Jessica C. Fares, Franziska E. Uhl, Danny D. Dinh, Jeffrey T. Kroetsch, Meghan Sauvé, Firhan A. Malik, Frank Matthes, Lotte Vanherle, Arman Adel, Abdul Momen, Hangjun Zhang, Roozbeh Aschar-Sobbi, Warren D. Foltz, Hoyee Wan, Manabu Sumiyoshi, R. Loch Macdonald, Mansoor Husain, Peter H. Backx, Scott P. Heximer, Anja Meissner, Steffen-Sebastian Bolz

Angaben zur Veröffentlichung / Publication details:

Lidington, Darcy, Jessica C. Fares, Franziska E. Uhl, Danny D. Dinh, Jeffrey T. Kroetsch, Meghan Sauvé, Firhan A. Malik, et al. 2019. "CFTR therapeutics normalize cerebral perfusion deficits in mouse models of heart failure and subarachnoid hemorrhage." *JACC: Basic to Translational Science* 4 (8): 940–58. https://doi.org/10.1016/j.jacbts.2019.07.004.

JACC: BASIC TO TRANSLATIONAL SCIENCE VOL. 4, NO. 8, 2019

PRECLINICAL RESEARCH

CFTR Therapeutics Normalize Cerebral Perfusion Deficits in Mouse Models of Heart Failure and Subarachnoid Hemorrhage

Darcy Lidington, PhD,[a,b,*] Jessica C. Fares, MSc,[a,b,*] Franziska E. Uhl, PhD,[c] Danny D. Dinh, MSc,[a,b] Jeffrey T. Kroetsch, PhD,[a,b] Meghan Sauvé, PhD,[a,b] Firhan A. Malik, PhD,[a] Frank Matthes, PhD,[c] Lotte Vanherle, MSc,[c] Arman Adel, BSc,[a] Abdul Momen, MD, PhD,[d] Hangjun Zhang, MD,[a,b] Roozbeh Aschar-Sobbi, PhD,[e] Warren D. Foltz, PhD,[f] Hoyee Wan, BSc,[g,h,i] Manabu Sumiyoshi, MD,[h,j] R. Loch Macdonald, MD, PhD,[g,h] Mansoor Husain, MD,[a,d,k,l] Peter H. Backx, PhD, DVM,[e,m] Scott P. Heximer, PhD,[a,k] Anja Meissner, PhD,[a,c,†] Steffen-Sebastian Bolz, MD, PhD[a,b,k,†]

VISUAL ABSTRACT

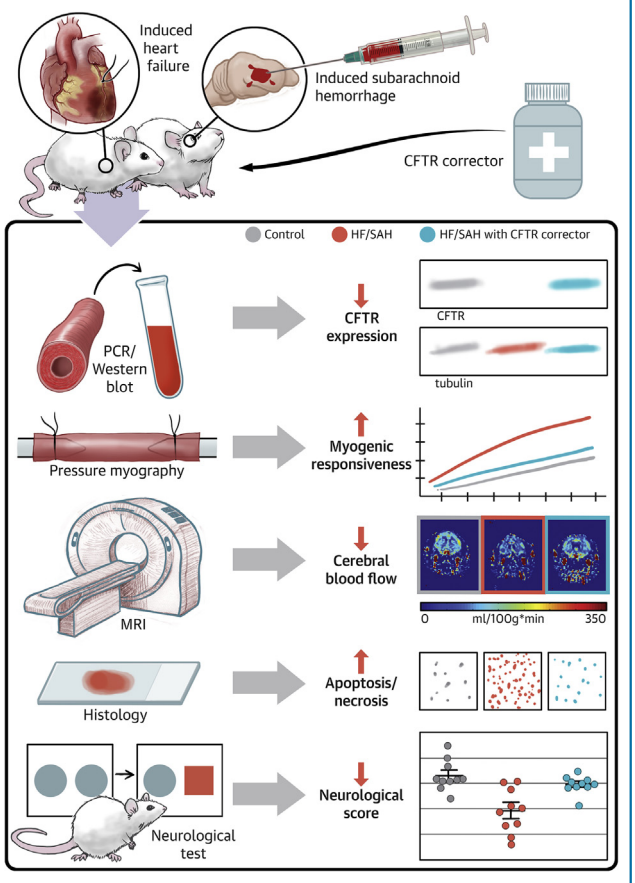

Lidington, D. et al. J Am Coll Cardiol Basic Trans Science. 2019;4(8):940-58.

ISSN 2452-302X https://doi.org/10.1016/j.jacbts.2019.07.004

HIGHLIGHTS

- **The cystic fibrosis transmembrane conductance regulator (CFTR) is a significant modulator of cerebrovascular reactivity; the loss of CFTR function enhances myogenic vasoconstriction.**
- **Heart failure and subarachnoid hemorrhage downregulate cerebrovascular CFTR protein expression; this leads to enhanced cerebral artery vasoconstriction, reduced cerebral perfusion, neuronal injury, and ultimately, neurologic deficits.**
- **CFTR therapeutics that maintain CFTR expression normalize the perfusion deficits, reduce neuronal injury, and improve neurologic function in these pathological settings.**

SUMMARY

Heart failure (HF) and subarachnoid hemorrhage (SAH) chronically reduce cerebral perfusion, which negatively affects clinical outcome. This work demonstrates a strong relationship between cerebral artery cystic fibrosis transmembrane conductance regulator (CFTR) expression and altered cerebrovascular reactivity in HF and SAH. In HF and SAH, CFTR corrector compounds (C18 or lumacaftor) normalize pathological alterations in cerebral artery CFTR expression, vascular reactivity, and cerebral perfusion, without affecting systemic hemodynamic parameters. This normalization correlates with reduced neuronal injury. Therefore, CFTR therapeutics have emerged as valuable clinical tools to manage cerebrovascular dysfunction, impaired cerebral perfusion, and neuronal injury. (J Am Coll Cardiol Basic Trans Science 2019;4:940–58)

ABBREVIATIONS AND ACRONYMS

CBF = cerebral blood flow

CFTR = cystic fibrosis transmembrane conductance regulator

HF = heart failure

MAP = mean arterial pressure

MOPS = 3-morpholinopropanesulfonic acid

MRI = magnetic resonance imaging

NIH = National Institutes of Health

PCA = posterior cerebral artery

SAH = subarachnoid hemorrhage

S1P = sphingosine-1-phosphate

TNF = tumor necrosis factor

TPR = total peripheral resistance

Survival rates for heart attack and stroke victims have significantly improved over the last 40 years. However, the extended longevity is frequently accompanied by cognitive decline. Cognitive impairment accelerates disease progression, reduces treatment compliance, progressively limits therapeutic treatment options, and imposes a substantial socioeconomic burden (1). Thus, cognitive

From the [a]Department of Physiology, University of Toronto, Toronto, Ontario, Canada; [b]Toronto Centre for Microvascular Medicine at The Ted Rogers Centre for Heart Research Translational Biology and Engineering Program, University of Toronto, Ontario, Canada; [c]Wallenberg Center for Molecular Medicine and Department of Experimental Medical Science, Lund University, Lund, Sweden; [d]Division of Cell & Molecular Biology, Toronto General Hospital Research Institute, Toronto, Ontario, Canada; [e]Division of Cardiology, University Health Network, Toronto, Ontario, Canada; [f]STTARR Innovation Centre, Department of Radiation Oncology, Princess Margaret Hospital, Toronto, Ontario, Canada; [g]Labatt Family Centre of Excellence in Brain Injury and Trauma Research, Keenan Research Centre for Biomedical Research and Li Ka Shing Knowledge Institute, St. Michael's Hospital, Toronto, Ontario, Canada; [h]Division of Neurosurgery, St. Michael's Hospital, and Department of Surgery, University of Toronto, Toronto, Ontario, Canada; [i]Sunnybrook Research Institute, Physical Sciences Platform and Department of Medical Biophysics, University of Toronto, Toronto, Ontario, Canada; [j]Institute of Health Biosciences, Department of Neurosurgery, University of Tokushima Graduate School, Tokushima, Japan; [k]Heart & Stroke/Richard Lewar Centre of Excellence for Cardiovascular Research, University of Toronto, Toronto, Ontario, Canada; [l]Department of Medicine, University of Toronto, Toronto, Ontario, Canada; and the [m]Department of Biology, York University, Toronto, Ontario, Canada. *Dr. Lidington and Ms. Fares contributed equally to this work and are joint first authors. †Drs. Meissner and Bolz contributed equally to this work and are joint senior authors. Dr. Kroetsch was supported by a Queen Elizabeth II/Heart & Stroke Foundation of Ontario Graduate Scholarship in Science and Technology. Dr. Sauvé was supported by Canadian Institutes of Health Research (CIHR) Doctoral Research Award and by Natural Sciences and Engineering Research Council (NSERC) of Canada. Dr. Dinh was supported by a NSERC MATCH scholarship. Dr. Malik was supported by a PGS-D doctoral scholarship. Dr. Backx was supported by the Canadian Institutes of Health Research (CIHR) (PJT 153159). Dr. Heximer was supported by CIHR (MOP-106670). Dr. Meissner was supported by the Swedish Science Council (VR 2017-01243), the Åke Wibergs Stiftelse (M17-0031), the Knut & Alice Wallenberg Foundation (2015.0030), and Lund University. Dr. Bolz was supported by the Operating and Infrastructure Grants from the Heart and Stroke Foundation of Ontario (HFSO) (G13-0002610 and G16-00014175) and CIHR (PJT 153269); a HSFO Career Investigator Award (CI-7432) and Mid-Career Investigator Award; the Brain Aneurysm Foundation (Northwell Health - North Shore University Hospital Brain Aneurysm Centre Chair of Research Award); the Canadian Foundation for Innovation and Ontario Research Fund (11810); and research support from the University of Toronto. Dr. Macdonald is chief scientific officer of Edge Therapeutics, Inc. All other authors have reported that they have no relationships relevant to the contents of this paper to disclose.

The authors attest they are in compliance with human studies committees and animal welfare regulations of the authors' institutions and Food and Drug Administration guidelines, including patient consent where appropriate. For more information, visit the *JACC: Basic to Translational Science* author instructions page.

Manuscript received April 29, 2019; revised manuscript received July 15, 2019, accepted July 16, 2019.

decline has emerged as a major clinical concern for patients with heart failure (HF) and stroke. Therefore, improving cognitive function will positively affect the primary disease, in addition to yielding both personal and socioeconomic benefits.

Our recent work focused on 2 etiologically distinct pathologies that are strongly associated with cognitive impairment: heart failure (HF) and subarachnoid hemorrhage (SAH). Clinically, the prevalence of early-onset cognitive impairment in patients with HF ranges from 25% to 75% (2); the prevalence in SAH is estimated to be 73% (3). Experimental mouse models emulate several key features of these diseases, including reduced cerebral blood flow (CBF) and compromised neurologic function (2,4-7). Despite their distinct etiologies, a common microvascular mechanism contributes to the reduced cerebral perfusion observed in experimental HF and SAH: an increase in cerebral artery myogenic reactivity, and hence, resistance to blood flow (5,6,8).

At the molecular level, both pathologies induce robust tumor necrosis factor (TNF) expression within the cerebral artery wall; this smooth muscle cell–localized TNF acts by an autocrine and/or paracrine mechanism to increase the bioavailability of sphingosine-1-phosphate (S1P), a pro-constrictive mediator that augments myogenic reactivity (4,6,8). Specifically, TNF signaling in cerebral arteries stimulates S1P production and concomitantly downregulates a critical negative regulator of S1P signaling, the cystic fibrosis transmembrane conductance regulator (CFTR) (8-10). CFTR acts as a negative regulator, because it sequesters S1P from its receptors and transports it across the plasma membrane for intracellular degradation (8). Therefore, reduced CFTR activity increases S1P bioavailability and represents a key component of the pathological augmentation of cerebral artery myogenic tone in HF and SAH (4,6,8).

SEE PAGE 959

Antagonizing TNF signaling with etanercept successfully abolishes the pathological augmentation of cerebrovascular vasoconstriction in HF and SAH, and thus, improves cerebral perfusion (4,6,8). This intervention also reduces neuronal injury and improves neuro-functional outcome (5,6), which strongly suggests that cerebral hypoperfusion contributes to the neurologic injury observed in these 2 models. However, as a clinical intervention, etanercept carries significant adverse effect risks stemming from immunosuppression (11) and potential effects on blood pressure control (12).

Based on our previous observations that 1) cerebral artery CFTR expression is reduced in HF and SAH (6,8); and 2) antagonizing TNF signaling in these pathologies normalizes CFTR expression concomitantly with vascular reactivity (6,8), we propose that CFTR represents a good therapeutic target for improving perturbed microvascular reactivity in HF and SAH and hence, CBF and cognitive decline. Food and Drug Administration–approved medications that increase CFTR expression and/or activity are available (13), and they are not generally associated with adverse side effects.

METHODS

The present investigation acquired the CFTR corrector therapeutic "C18" and the anti-human CFTR antibody (designated "596") through the Cystic Fibrosis Foundation Therapeutics Chemical and Antibody Distribution Programs. All other reagents used in this investigation are commercially available and are listed in the Supplemental Appendix.

ANIMALS. The Institutional Animal Care and Use Committees at the University of Toronto and the University Health Network approved all animal care and experimental protocols. Commercially available male wild-type mice (2 to 3 months; C57BL/6N) were purchased from Charles River Laboratories (Montreal, Quebec, Canada). Male mice homozygous for the ΔF508 CFTR mutation ($CFTR^{tm1EUR}$; designated "ΔF508" in the present study) (14), CFTR gene deletion ($CFTR^{tm1Unc}$; designated $CFTR^{-/-}$) and the complimentary wild-type control littermates were obtained from an established colony at the Hospital for Sick Children (Toronto, Ontario, Canada) (all $CFTR^{-/-}$, $CFTR^{\Delta F508}$, and wild-type littermates are mixed strains). Phenotype details for these CFTR mutant mice can be found in the Supplemental Appendix. All mice were housed under a standard 14 h/10 h light–dark cycle, fed normal chow, and had access to water *ad libitum*.

MYOCARDIAL INFARCTION. HF was induced by surgical ligation of the left anterior descending coronary artery (4). Briefly, mice were anesthetized with isoflurane, intubated with a 20-gauge angiocatheter, and ventilated with room air. Under sterile conditions, the thorax and pericardium were opened, and the left anterior descending coronary artery was permanently ligated with 7-0 silk suture (Deknatel; Fall River, Massachusetts). In sham-operated control mice, the thorax and pericardium were opened, but the left anterior descending coronary artery was not ligated. Following the procedure, the chest was

closed, and the mice were extubated upon spontaneous respiration. All experimental measurements in the HF model were conducted at or after 6 weeks post-infarction. Our previous work demonstrated that the cardiac injury is stable after 6 weeks, and thus, treatments do not alter and/or improve cardiac function (4). This allowed us to unambiguously attribute improvements in CBF in this model to a cerebrovascular mechanism.

INDUCTION OF SAH. We used a well-characterized model of experimental SAH (6). Briefly, each mouse was anesthetized (isoflurane), and its head was fixed in a stereotactic frame; a 7-mm incision was made along the midline of the anterior scalp and a 0.9-mm hole drilled into the skull 4.5-mm anterior to the bregma. A spinal needle was advanced to the chiasmatic cistern; 80 μl of arterial blood was injected into the intracranial space over 10 s. The injected blood was obtained from a separate wild-type donor mouse (via cardiac puncture) immediately before injection and did not contain anticoagulants. Following injection, the scalp incision was closed. Buprenorphine (0.05 mg/kg; 0.5 to 1.0 ml volume) was administered twice a day for 2 days (initiated immediately following the SAH surgical procedure). Sham-operated animals underwent an identical surgical procedure, with sterile saline injected instead of blood. All experimental measurements in the SAH model were conducted at 2 days post-SAH induction. Our previous work demonstrated that SAH maximally augments myogenic tone at this time point; reductions in CBF, neuronal injury, and compromised neurologic function are also evident at this time (6).

ISOLATION AND FUNCTIONAL ASSESSMENT OF RESISTANCE ARTERIES. Mouse olfactory (a first branch of the anterior cerebral artery) and posterior cerebral arteries (PCAs) were carefully dissected, cannulated onto micropipettes, stretched to their in vivo lengths, and pressurized to 45 mm Hg, as previously described (4,6). Mouse skeletal muscle resistance arteries were dissected from the cremaster muscle, cannulated, and pressurized to 60 mm Hg. All functional experiments were conducted in 3-morpholinopropanesulfonic acid (MOPS) buffered saline at 37°C with no perfusion. Vasomotor responses to phenylephrine (5 μmol/l for PCAs, 10 μmol/l for cremaster skeletal muscle arteries) provided an assessment of vessel viability at the beginning and end of each experiment. Arteries that failed to show ≥25% constriction to phenylephrine were excluded.

Myogenic responses were elicited by stepwise 20 mm Hg increases in transmural pressure from 20 to 80 mm Hg (olfactory arteries) or 100 mm Hg (PCAs and cremaster skeletal muscle resistance arteries). At each pressure step, vessel diameter (dia_{active}) was measured once a steady state was reached (5 min). Vessels that required treatment [e.g., $CFTR_{(inh)}$-172] were incubated with the reagent in MOPS for 30 min, and myogenic responses were then assessed in the presence of that reagent. Following completion of all dia_{active} measurements, MOPS buffer was replaced with a calcium-free version and maximal passive diameter (dia_{max}) was recorded at each pressure step.

Myogenic tone was calculated as the percent constriction in relation to the maximal diameter at each respective transmural pressure: tone (% of dia_{max}) = $[(dia_{max} - dia_{active})/dia_{max}] \times 100$, where dia_{active} was the vessel diameter in MOPS containing calcium and dia_{max} was the diameter in calcium-free MOPS. Analyses of vasomotor responses to phenylephrine used the same calculation, only in this case, dia_{active} represented the vessel diameter at steady state following application of the given agent and dia_{max} represented the maximal diameter measured under calcium-free conditions.

GLOBAL HEMODYNAMIC PARAMETERS. Echocardiographic measurements were collected with a 30-MHz mechanical sector transducer (Vevo 770; Visual Sonics, Toronto, Ontario, Canada) in conjunction with the mean arterial pressure (MAP) measurements (SPR-671 micro-tip mouse pressure catheter; Millar Inc., Houston, Texas) as previously described (4,8). Measurements and calculations are described in the Supplemental Appendix.

MAGNETIC RESONANCE IMAGING–BASED CEREBRAL BLOOD FLOW MEASUREMENTS. We used a noninvasive cardiac magnetic resonance imaging (MRI) approach (Flow-sensitive Alternating Inversion Recovery [FAIR] technique) to evaluate cerebral perfusion, as previously described (6). Briefly, the FAIR technique isolates perfusion as an accelerated T_1 signal relaxation. MRI signals (Biospec 70/30 USR; Bruker Corporation, Ettlingen, Germany) were acquired from vertical sections of the fore-, mid-, and hind-brain, which correspond to the anterior, mixed, and posterior circulations. FAIR images were evaluated for designated regions of interest (region placement is displayed in Supplemental Figure 1) using standardized algorithms and image processing procedures (MIPAV; National Institutes of Health [NIH], Bethesda, Maryland; http://mipav.cit.nih.gov). The procedures are described in detail in the Supplemental Appendix.

FIGURE 1 CBF Is Reduced in CFTRΔF508 Mice

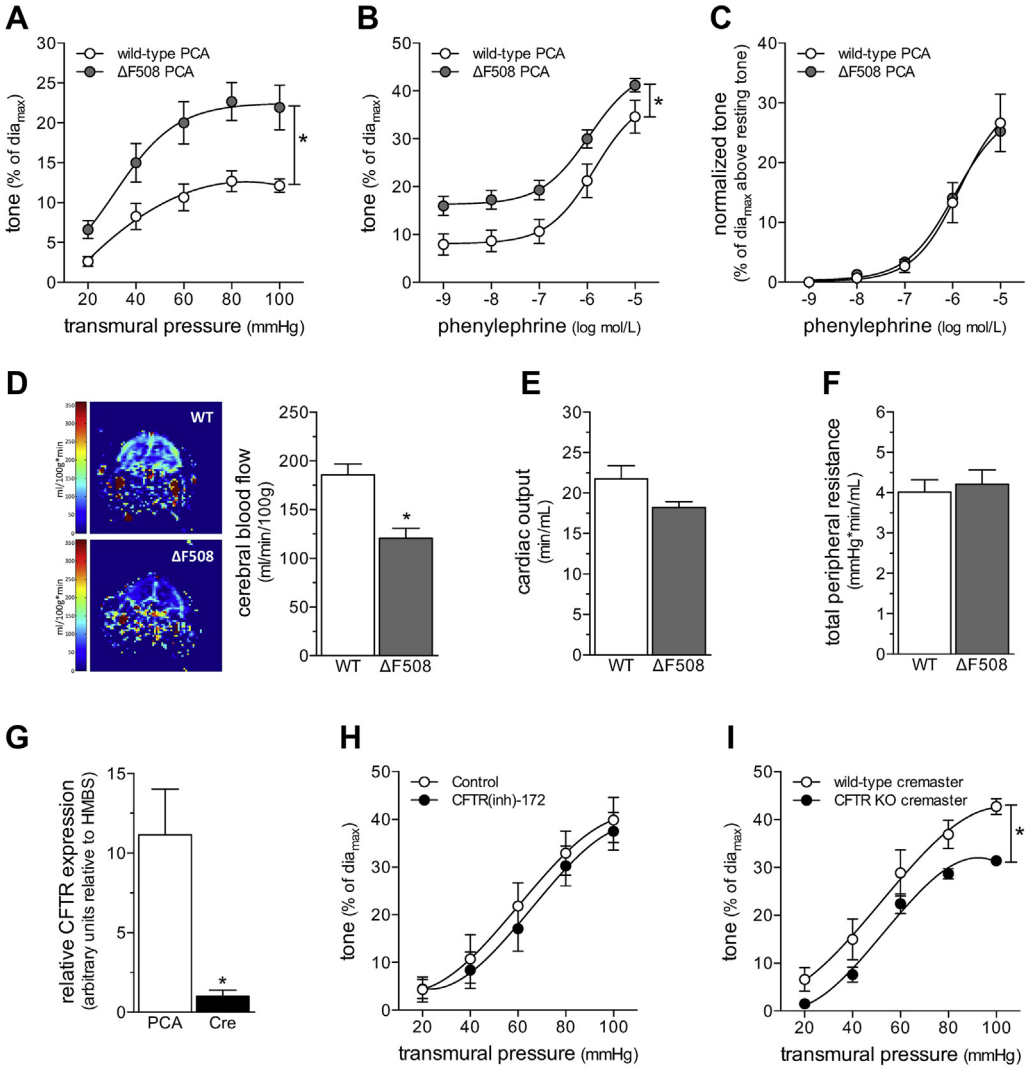

(A) Myogenic vasoconstriction is stronger in posterior cerebral arteries (PCAs) isolated from cystic fibrosis transmembrane conductance regulator (CFTR) ΔF508 mutant mice, relative to wild-type (WT) littermate control mice. **(B)** PCAs isolated from $CFTR^{\Delta F508}$ mice display an upward shift in their phenylephrine dose–response relationship. **(C)** However, once the phenylephrine responses are normalized to basal tone ($tone_{active} - tone_{rest}$, where $tone_{active}$ is the tone at given phenylephrine concentration and $tone_{rest}$ is the tone immediately before stimulation), the WT and $CFTR^{\Delta F508}$ phenylephrine dose–response relationships are virtually identical. Mean maximal vessel diameters at 45 mm Hg (dia_{max}) are: $CFTR^{\Delta F508}$: 186 ± 2 μm; n = 6 from 4 mice, and WT: 169 ± 8 μm; n = 5 from 3 mice (*t*-test: p = NS for dia_{max}). **(D)** Magnetic resonance imaging was used to measure cerebral blood flow in predefined forebrain cortical regions. Representative perfusion maps from WT and $CFTR^{\Delta F508}$ mouse forebrains are shown. Cerebral blood flow (CBF) is significantly lower in $CFTR^{\Delta F508}$ mice (n = 10), relative to WT littermates (n = 11); however, neither **(E)** cardiac output (n = 5 for both groups) nor **(F)** total peripheral resistance (n = 5 for both groups) differed between the 2 genotypes. **(G)** In WT mice, CFTR mRNA expression is significantly higher in PCAs (n = 5), relative to cremaster skeletal muscle arteries (Cre) (n = 6). **(H)** Cre myogenic tone is not altered by CFTR inhibition in vitro (100 nmol/l $CFTR_{(inh)}$-172 for 30 min). **(I)** However, CFTR gene deletion (CFTR KO) induces a modest, but significant attenuation of myogenic tone. Mean maximal vessel diameters at 60 mm Hg (dia_{max}) are **(G)** WT: 72 ± 3 μm, n = 5 from 4 mice; **(H)** CFTR knock out (KO): 88 ± 4 μm, n = 6 from 4 mice; and **(H)** WT littermates: 78 ± 4 μm, n = 5 from 2 mice. All data are mean ± SEM. In **(A to C, H, and I)**, *p < 0.05 for unpaired comparisons with a 2-way analysis of variance; in **(D to G)**, *p < 0.05 for unpaired comparisons with a *t*-test.

FIGURE 2 **C18 increases WT CFTR Protein Expression and Function by a Proteostatic Mechanism**

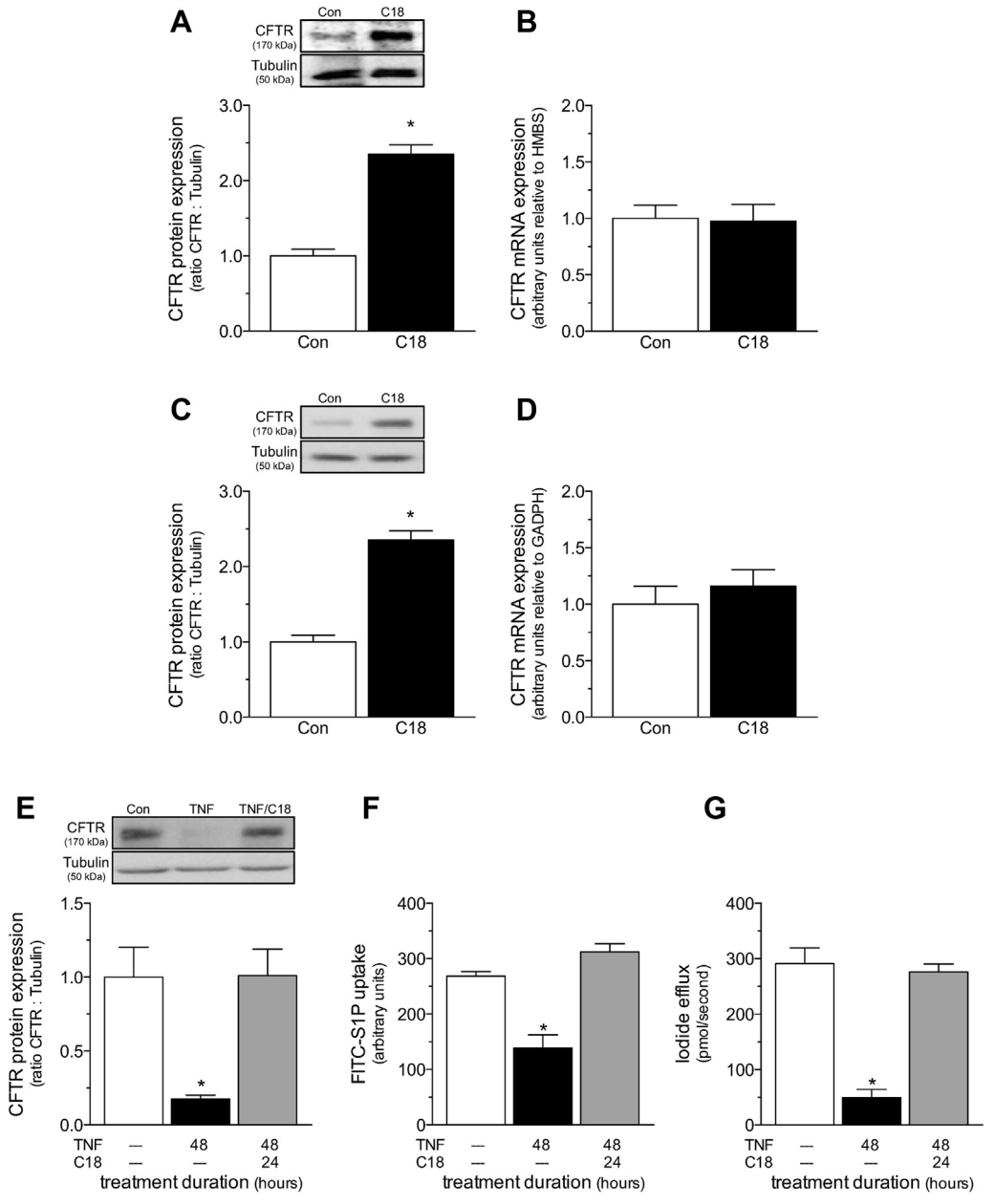

(A) Cerebral arteries isolated from naïve mice treated with C18 (3 mg/kg intraperitoneally daily for 2 days; n = 5) have higher CFTR protein expression than arteries collected from vehicle control (Con) mice (n = 5). **(B)** C18 does not influence cerebral artery CFTR mRNA expression (Con: n = 6; C18: n = 5). **(C)** C18 (6 μmol/l; 24 h) increases CFTR protein expression in baby hamster kidney fibroblast cells stably expressing human CFTR (n = 12 for both groups). **(D)** C18 does not influence CFTR mRNA expression in this system (n = 6 for both groups). **(E)** Tumor necrosis factor (TNF) (10 ng/ml for 48 h) downregulates CFTR protein expression in mesenteric artery primary vascular smooth muscle cells (Con: n = 8; TNF: n = 8); co-incubating TNF with C18 (6 μmol/l; 24 h) following 24 h TNF incubation (i.e., 48 h TNF + 24 h C18) fully restores CFTR protein expression (n = 7). The restoration of CFTR protein expression in vascular smooth muscle cells correlates with the normalization of attenuated **(F)** Fluorescein isothiocyanate-labeled sphingosine-1-phosphate (FITC-S1P) uptake (measured as an increase in fluorescence intensity at 525 nm by a standard fluorescence-activated cell sorting analysis technique; Con: n = 7; TNF: n = 10; TNF+C18: n = 6) and **(G)** forskolin-stimulated iodide efflux (Con: n = 7; TNF: n = 6; TNF+C18: n = 6). All data are mean ± SEM. In **(A to D)**, *p < 0.05 for an unpaired comparison with a *t*-test; in **(E to G)**, *p < 0.05 for unpaired comparisons to the Con mice with a 1-way analysis of variance and Tukey's post hoc test. Other abbreviation as in Figure 1.

FIGURE 3 C18 Restores Cerebral Perfusion in HF

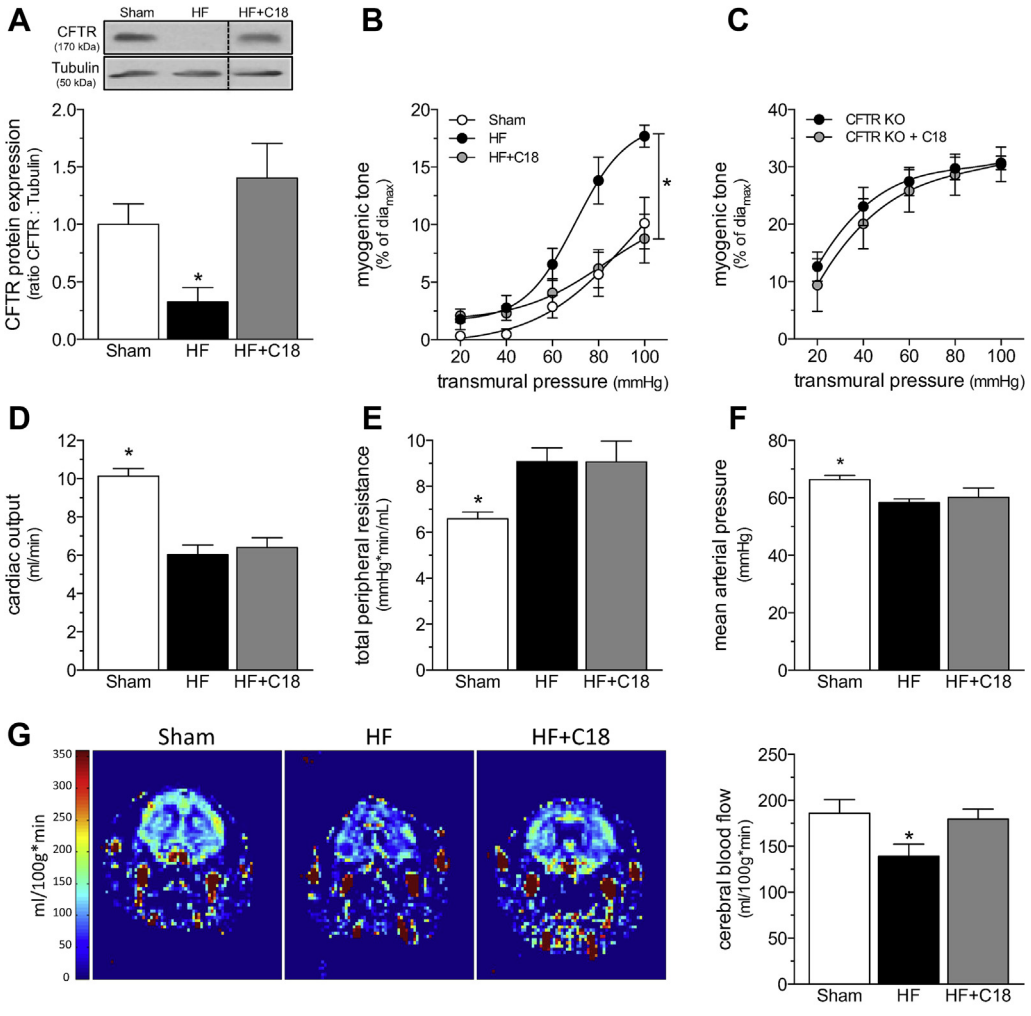

(A) Cerebral arteries isolated from mice with HF (6 weeks post-left anterior descending coronary artery ligation) have reduced CFTR protein expression (n = 5) relative to arteries isolated from sham-operated controls (n = 6). C18 treatment in vivo (3 mg/kg intraperitoneally daily for 2 days) eliminates this reduction in cerebral artery CFTR protein expression (n = 8). **(B)** C18 treatment in vivo reduces myogenic tone in PCAs isolated from HF mice, an effect **(C)** not observed in PCAs isolated from CFTR KO mice. Mean maximal vessel diameters at 45 mm Hg (dia_{max}) are sham: 146 ± 9 μm; n = 5 from 3 mice; HF: 149 ± 8 μm; n = 6 from 4 mice; HF+C18: 155 ± 8 μm; n = 8 from 6 mice (1-way analysis of variance: p = NS); and CFTR KO: 142 ± 5 μm; n = 6 from 3 mice; CFTR KO+C18: 145 ± 5 μm; n = 6 from 3 mice (Student's *t*-test: p = NS). Relative to sham-operated control mice, mice with HF have **(D)** reduced cardiac output (sham: n = 6; HF: n = 8; HF+C18: n = 8), **(E)** elevated total peripheral resistance (n = 6 for all groups), and **(F)** reduced mean arterial pressure (n = 6 for all groups); C18 treatment did not affect these parameters in mice with HF. **(G)** Representative magnetic resonance perfusion maps that were used to determine forebrain cortical cerebral blood flow. HF stimulated a reduction in cerebral perfusion, and C18 treatment significantly improved cerebral perfusion in mice with HF (sham: n = 6; HF: n = 8; HF+C18: n = 8). All data are mean ± SEM. For **(A and G)**, *p < 0.05 for unpaired comparisons to the sham with a 1-way analysis of variance and Dunnett's post hoc test; for **(B)**, *p < 0.05 for unpaired comparisons to sham with a 2-way analysis of variance and Tukey's post hoc test; in **(C)**, groups were statistically compared with a 2-way analysis of variance (p = NS); and in **(D to F)**, *p < 0.05 for unpaired comparisons to HF with a 1-way analysis of variance and Dunnett's post hoc test. All samples in the representative Western blot image displayed in **(A)** originated from the same film, but the HF+C18 sample was not adjacently positioned on this film, as shown in this Figure. Abbreviations as in Figures 1 and 3.

MRI-BASED EDEMA MEASUREMENT. Edema was assessed by quantitative T_2 mapping (15), using a 7-T micro-MRI system (Biospec 70/30 USR; Bruker Corporation). The T_2 mapping acquisition generated quantitative T_2 maps in 9 contiguous 2-dimensional axial slices, with 1 mm thickness, covering the volume from the fore-brain through to the hind-brain. T_2 maps were generated from

FIGURE 4 **C18 Does Not Induce Cerebral Edema**

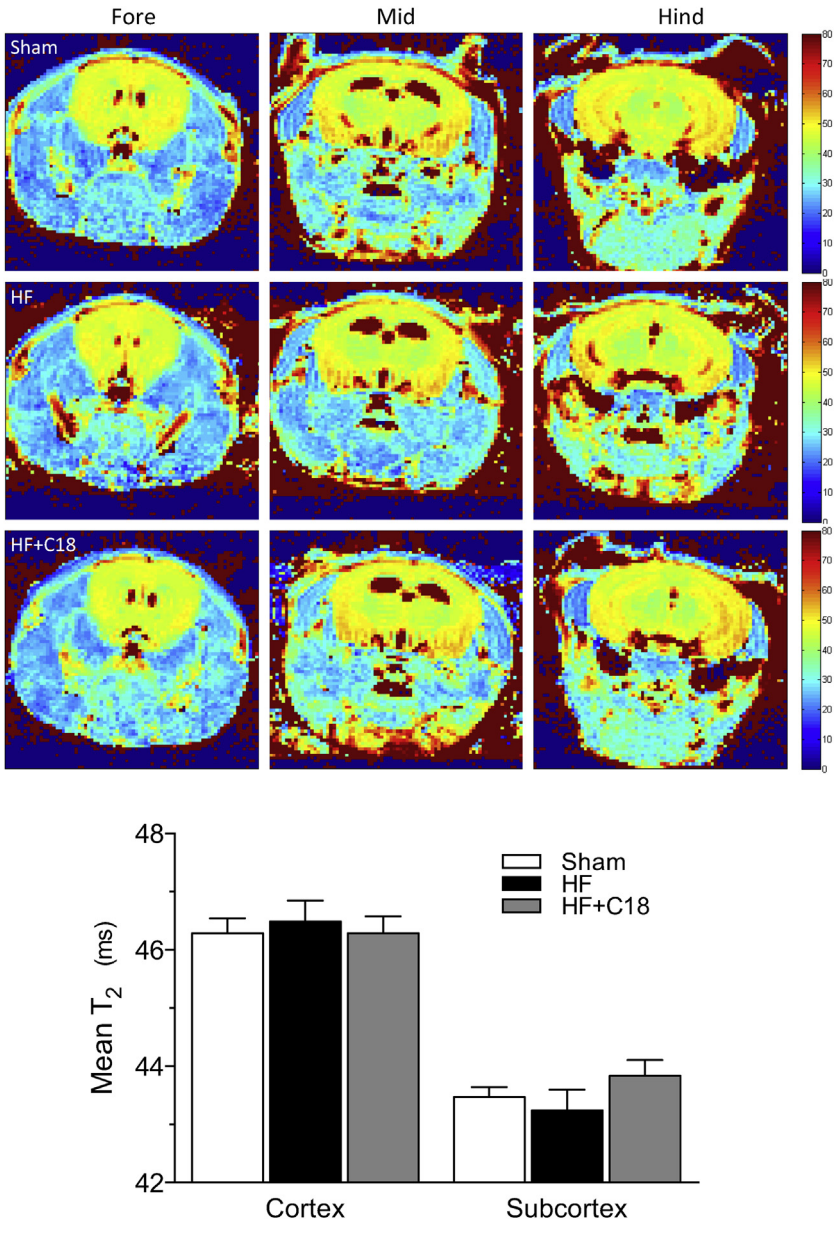

Representative quantitative T_2 maps that assess brain water content as T_2 relaxation times in magnetic resonance images. A total of 9 T_2 maps were assessed per mouse, which cover the fore-, mid-, and hind-brain regions. The representative images display slices from the **(left)** fore-, **(center)** mid-, and **(right)** hind-brain regions of **(top)** sham, **(middle)** HF, and **(bottom)** C18-treated (3 mg/kg intraperitoneally daily for 2 days) HF mice. Neither HF nor C18 treatment in HF mice induced an alteration in the T_2 relaxation times in any region of interest within any of the slices assessed. The data were therefore pooled to yield a mean T_2 relaxation time for the cortical and subcortical region and graphically presented (sham: n = 7; HF: n = 7; HF+C18: n = 6). All data are mean ± SEM. Groups were statistically compared with a 1-way analysis of variance test (p = NS among the sham, HF, and HF+C18 groups in the cortical and subcortical regions, respectively). Abbreviations as in Figure 1.

T_2-weighted images at echo times from 12 to 384 ms, using inline Bruker software, via linear regression of the logarithmically transformed signal magnitudes and the echo times on a per voxel basis. The T_2 values were extracted using MIPAV software, using manually drawn regions of interest placed within the fore-, middle- and hind-brain T_2 maps.

FIGURE 5 C18 Improves Neuronal Morphology and Neuronal Function in HF

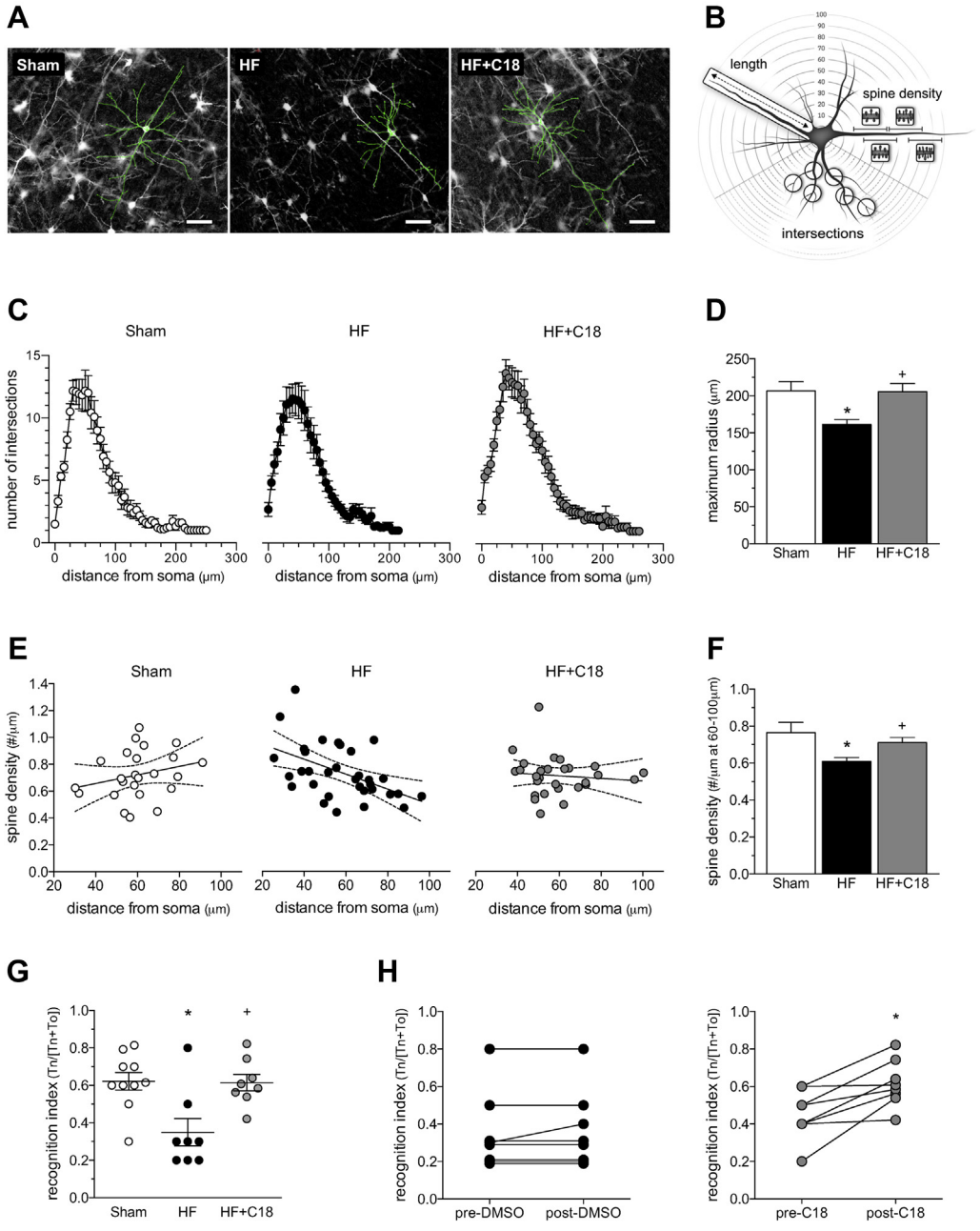

Continued on the next page

CELL CULTURE AND MOLECULAR AND/OR BIOCHEMICAL ASSESSMENTS. We previously described the mesenteric artery smooth muscle and baby hamster kidney fibroblast cell systems and their culture conditions (8,16). Standard procedures were used for Western blots, real-time polymerase chain reaction, Fluorescein isothiocyanate labeled S1P (FITC-S1P) uptake, and iodide efflux measurements (6,8,16). Specific details are provided in the Supplemental Appendix.

FLUORESCENT IMMUNOHISTOCHEMISTRY AND FLUORO-JADE STAINING. Brains were cleared of blood and fixed via aortic perfusion with 4% paraformaldehyde; the brains were then dissected, and

coronal sections 1 mm posterior to the bregma were cut. We used standard procedures to prepare slides with 5-μm-thick cryostat slices and to complete the assessments of cleaved caspase-3 and Fluoro-Jade staining (6). Caspase-3 and Fluoro-Jade–positive cells were counted in the cortical region of coronal sections that included the left and right temporal and parietal lobes at 200× magnification (1 slice assessed per mouse). The procedures are described in detail in the Supplemental Appendix.

HISTOLOGICAL ANALYSIS OF DENDRITE MORPHOLOGY. Brains were cleared of blood and processed with a commercially available Rapid GolgiStain kit (FD NeuroTechnologies Inc.; Columbia, Maryland, USA), as previously described (5). Neurons and their dendritic networks were imaged using stereology-based NIS Elements AR software (Nikon Instruments Europe; Amsterdam, the Netherlands) and analyzed using Image J (NIH). The dendrite networks of single cortical pyramidal neurons from the frontal cortex were identified and digitally isolated from hyperstack images using the semi-automated Simple Neurite Tracer plugin for Image J; the traced images were subsequently analyzed by Sholl analysis (https://imagej.net/Sholl_Analysis, version 3.7.4). The procedures are described in greater detail in the Supplemental Appendix.

NEUROLOGIC FUNCTION IN SAH MICE. Neurologic function was assessed using the modified Garcia score, as previously described (6). The neurologic assessment consists of 6 domains: spontaneous activity, spontaneous movement of all 4 limbs, forepaw outstretching, climbing, body proprioception, and response to vibrissae touch. Two blinded observers conducted the neurologic assessment 2 days after SAH. The maximum score is 18, indicative of normal neurologic function.

COGNITIVE FUNCTION IN HF MICE. We used a well-established novel object recognition task to evaluate rhino-cortical nonspatial memory, as previously described (5,17). Briefly, habituated mice were exposed to 2 identical objects for 5 min. After a 5-min delay, 1 of the original objects was replaced with a novel object, and the mice were retested. The mice were video-tracked with AnyMaze software (Stoelting; Dublin, Ireland) that recorded the time spent interacting with the novel (Tn) and original (To) objects. A recognition index was calculated as the time spent interacting with the novel object versus the total time spent interacting with either object (Tn/[Tn+To]). The objects and arena were thoroughly cleaned with 70% ethanol between each test, to eliminate potential odor cues.

STATISTICAL ANALYSIS. All data are expressed as means ± SEM, where n is the number of independent measures (i.e., samples, vessels assessments, or experimental subjects). Data were statistically analyzed using Graphpad Prism 6 software (San Diego, California). For statistical comparisons, a Student's *t*-test was used for the comparison of 2 independent groups. For comparison of multiple independent groups, 1-way analysis of variance was used, followed by a Tukey's or Dunnett's post hoc test, as appropriate. For the assessment of myogenic responses and dose–response relationships, data were analyzed with a 2-way analysis of variance, followed by a Tukey's post hoc test. Differences were considered significant at $p < 0.05$. All histological and

FIGURE 5 Continued

(A) Representative images of Golgi-stained pyramidal neurons from sham mice, mice with heart failure (HF), and C18-treated HF mice (3 mg/kg intraperitoneally daily for 2 weeks; treatment initiated at 10 weeks post-infarction). The morphology of both the basal and apical dendrites is highlighted with traces superimposed onto the images. **(B)** The images displayed in **(A)** are quantitatively assessed by Sholl analysis, which characterizes the dendritic network at 5-μm intervals to a maximal radius of 300 μm away from soma. **(C)** Sholl analysis histograms plotting the number of dendrite intersections (i.e., dendritic branching) versus dendrite length (i.e., distance from neuronal soma) show no differences in branching morphology across the sham (n = 12 neurons from N = 4 mice), HF (n = 12; N = 4), and HF+C18 (n = 11; N = 4) groups. However, dendritic length is shorter in HF mice, relative to the sham and HF+C18 groups. Accordingly, **(D)** the mean dendrite length (i.e., maximum radius) is significantly reduced in HF mice relative to sham mice, an effect that is normalized by C18 treatment. **(E)** In sham mice (n = 11; N = 4), the spine density of basal dendrites is relatively consistent over the length of the dendrite, yielding a slope that is not statistically different from zero. In HF mice (n = 13; N = 4), a statistically significant ($p < 0.05$) negative slope is observed, indicating a loss of spine density within the distal regions of the dendrite; HF mice treated with C18 (n = 12; N = 4) do not possess the negative slope observed for HF mice. Consequently, **(F)** mean basal dendrite spine density 60 to 100 μm from soma is significantly reduced in HF mice relative to sham controls; this morphological difference is normalized by C18 treatment. **(G)** Relative to sham mice (N = 10), HF (N = 8) attenuates rhino-cortical–dependent, short-term retention of object familiarity in a nonspatial novel object recognition task, with a 5-min delay interval; the attenuation is not present in C18-treated HF mice (N = 8). **(H)** Longitudinal pre-/post-treatment analyses of the same vehicle- and C18- treated HF mice confirm a statistically significant C18 treatment effect on rhino-cortical, short-term retention memory. In **(D, F, and G),** *$p < 0.05$ for unpaired comparisons to the sham and +$p < 0.05$ for an unpaired comparison between the HF and HF+C18 groups with a 1-way analysis of variance and Tukey's post hoc test. In **(H)** *$p < 0.05$ for a comparison with a paired *t*-test. Tn = time spent interacting with novel object; To = time spent interacting with original object.

neurological/cognitive function data were collected under blinded conditions; all other data presented in this study did not require blinding and were not collected under blinded conditions.

RESULTS

DEFICIENT CFTR FUNCTION DRIVES REDUCED CEREBRAL PERFUSION. Our previous work demonstrated that CFTR prominently regulates cerebral artery myogenic tone and identified a strong correlation between cerebral artery CFTR protein expression and cerebral perfusion (6,8). Therefore, our mechanistic concept proposes that correcting deficient cerebrovascular CFTR activity (i.e., reduced S1P transport due to decreased CFTR expression at the cell surface) is a viable therapeutic strategy for normalizing compromised cerebral myogenic responsiveness, and hence, CBF (8).

To establish the causative link between cerebral artery CFTR activity and cerebral perfusion, we used CFTR mutant mice (described in detail in the Supplemental Appendix). Although CFTR mutant mice are smaller in size and have a strong propensity for bowel obstruction, they possess a relatively mild cystic fibrosis phenotype compared with humans: most organs, including the lower respiratory tract, appear histologically normal in the absence of challenge (18,19). Nevertheless, CFTR mutant mice in general, and $CFTR^{-/-}$ mice in particular, are known to adversely react to stress (18). In our hands, $CFTR^{-/-}$ mice were extremely sensitive to experimental stressors, which did not permit accurate and reproducible echocardiography and/or CBF measurements. $CFTR^{\Delta F508}$ mice, which have minimal cell surface CFTR expression and activity (14), were more stable. This underpinned our strategic decision to use $CFTR^{\Delta F508}$ mice for relating cerebral artery myogenic tone to hemodynamic parameters in a loss of function phenotype.

We assessed vasomotor reactivity in PCAs to directly compare the $CFTR^{\Delta F508}$ phenotype to our previously published characterization of PCA responses from CFTR knockout mice (8). As expected, PCAs from $CFTR^{\Delta F508}$ mice displayed augmented myogenic tone, relative to wild-type littermates (**Figure 1A**); the magnitude of the augmentation was qualitatively similar to that found for $CFTR^{-/-}$ mice (8). Phenylephrine responses displayed an upward shift due to the enhanced myogenic tone (**Figure 1B**); however, the EC_{50} values were not different (log EC_{50} wild type: -5.83 ± 0.21; $n = 5$ from 3 mice; log EC_{50} $CFTR^{\Delta F508}$: -6.00 ± 0.04; $n = 6$ from 4 mice; Student's *t*-test: $p = NS$), and the difference between the curves was eliminated by correcting for the difference in basal tone (i.e., myogenic tone at 45 mm Hg) (**Figure 1C**). Therefore, the ΔF508 mutation augmented myogenic responsiveness, but did not alter general contractility. CBF was significantly lower in $CFTR^{\Delta F508}$ mice (**Figure 1D**); however, neither cardiac output (**Figure 1E**) nor total peripheral resistance (TPR) (**Figure 1F**) were affected by the mutation (additional hemodynamic parameters are listed in Supplemental Table 1). Based on these observations, the cerebral perfusion deficit was clearly vascular in origin.

The $CFTR^{\Delta F508}$ mutation did not change TPR, indicating that not all vascular beds were subject to CFTR-dependent regulation. Because TPR is primarily generated and regulated by skeletal muscle resistance arteries (20), we assessed whether CFTR influenced myogenic tone in mouse cremaster skeletal muscle resistance arteries. CFTR mRNA expression was approximately 10-fold lower in wild-type mouse cremaster skeletal muscle resistance arteries, relative to cerebral arteries (**Figure 1G**). Inhibiting CFTR activity in vitro (100 nmol/; $CFTR_{(inh)}$-172, 30 min) did not affect wild-type cremaster artery myogenic tone (**Figure 1H**), which was in contrast to our recent observations that $CFTR_{(inh)}$-172 augmented olfactory cerebral artery myogenic tone (6). Unlike PCAs (8), CFTR gene deletion did not augment myogenic tone in cremaster skeletal muscle resistance arteries (**Figure 1I**); myogenic tone was mildly attenuated and corresponded to lower MAP (Supplemental Figure 2). Phenylephrine dose–response relationships were not altered by either CFTR inhibition in vitro or CFTR gene deletion (Supplemental Figure 3).

In summary, our $CFTR^{\Delta F508}$ experiments established: 1) a causative link between CFTR expression, PCA myogenic responsiveness, and CBF; 2) that CFTR modulates myogenic tone in specific vascular beds; and 3) that CFTR does not modulate skeletal muscle resistance artery tone, which was notable, because these arteries prominently contribute to TPR. Because HF and SAH downregulate cerebral artery CFTR expression concomitant with microvascular dysfunction (6,8), these data provide a strong mechanistic foundation for using CFTR-modulating medications to specifically correct cerebrovascular dysfunction and CBF deficits in this pathological setting.

C18 INCREASES CFTR ACTIVITY FOLLOWING TNF-DEPENDENT DOWN-REGULATION. Current CFTR-modulating medications, identified via high-throughput drug screens, are experimentally and clinically used to mitigate the effects of cystic fibrosis. CFTR therapeutics are broadly segregated

FIGURE 6 C18 Restores Cerebral Perfusion In SAH

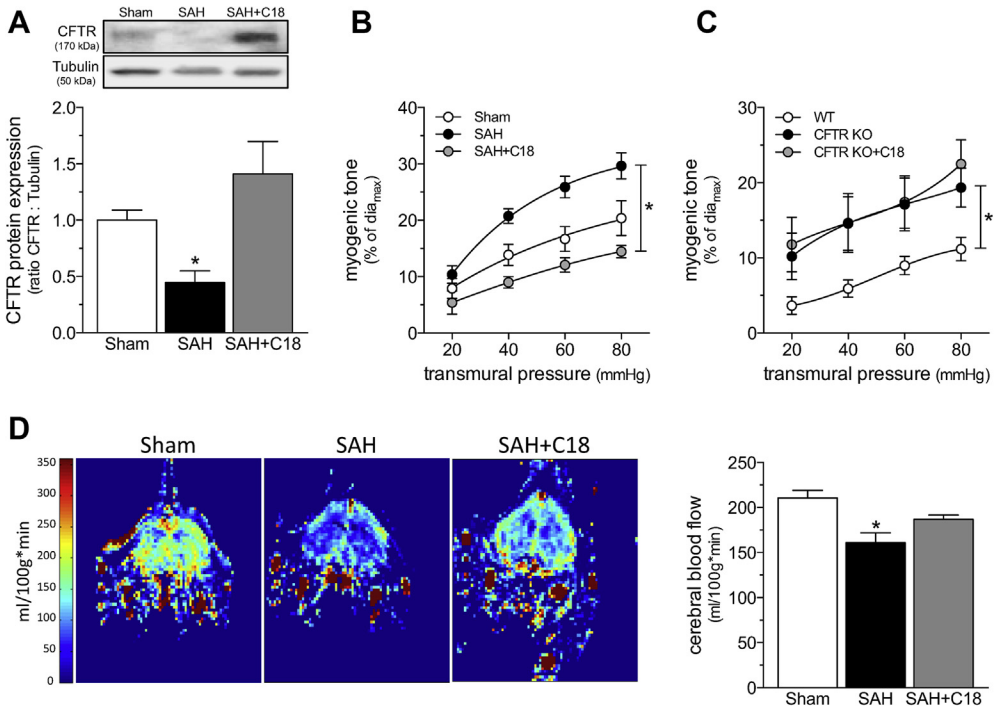

(A) Cerebral arteries isolated from mice with SAH (2 days post-SAH induction) have reduced CFTR protein expression (n = 6), relative to arteries isolated from sham-operated controls (n = 6). C18 treatment in vivo (3 mg/kg intraperitoneally daily for 2 days) eliminated this reduction in artery CFTR protein expression (n = 6). **(B)** C18 treatment in vivo reduced myogenic tone in olfactory arteries isolated from mice with SAH, an effect **(C)** not observed in olfactory arteries isolated from CFTR KO mice. Mean maximal vessel diameters at 45 mmHg (dia_{max}) are sham: 113 ± 3 μm; n = 5 from 3 mice; SAH: 109 ± 6 μm; n = 6 from 6 mice; SAH+C18:104 ± 12 μm; n = 5 from 4 mice (1-way analysis of variance: p = NS); and CFTR WT: 98 ± 6 μm; n = 8 from 4 mice; CFTR KO: 110 ± 8 μm; n = 5 from 4 mice; CFTR KO+C18: 96 ± 6 μm; n = 6 from 3 mice (1-way analysis of variance: p = NS). **(D)** Representative magnetic resonance perfusion maps that were used to determine forebrain cortical CBF. SAH stimulated a reduction in cerebral perfusion; C18 treatment significantly improved cerebral perfusion in mice with SAH (sham: n = 10; SAH: n = 5; SAH+C18: n = 9). All data are mean ± SEM. In **(A and D)**, *p < 0.05 for unpaired comparisons to the sham with a 1-way analysis of variance and Dunnett's post hoc test. In **(B)**, *p < 0.05 for unpaired comparisons to SAH with a 2-way analysis of variance and Tukey's post hoc test. In **(C)**, *p < 0.05 for unpaired comparisons to WT with a 2-way analysis of variance and Tukey's post hoc test. Abbreviations as in Figures 1, 3, and 4.

into 2 distinct classes: CFTR potentiators (which increase CFTR channel activity) and CFTR correctors (which increase CFTR cell surface expression). Because CFTR potentiators (e.g., ivacaftor) display limited efficacy when CFTR abundance is low, we selected a CFTR corrector for our intervention. In this regard, we used the experimental CFTR corrector C18 based on the previous demonstration that it directly interacts with and stabilizes wild-type CFTR, thereby increasing CFTR expression at the plasma membrane (21).

We first confirmed that C18 is capable of increasing both mouse and human CFTR expression. Cerebral arteries isolated from naïve mice injected with C18 (3 mg/kg intraperioneally daily for 2 days) displayed higher CFTR protein expression levels, relative to vehicle-treated control mice (Figure 2A); CFTR mRNA expression was not affected by C18 (Figure 2B). To confirm C18's effect on human CFTR, we used a heterologous expression system of baby hamster kidney fibroblast cells that stably expressed a human CFTR construct. C18 treatment (6 μmol/l; 24 h) more than doubled CFTR protein expression in baby hamster kidney fibroblast cells (Figure 2C), but had no effect on CFTR mRNA expression in this system (Figure 2D). Collectively, the data are consistent with previous observations that C18 exerts direct stabilizing effects on CFTR protein expression (21) and demonstrates its efficacy against both murine and human CFTR.

We next assessed whether C18 treatment increases CFTR abundance in a cell culture setting that modeled the relevant pathophysiological mechanisms and cellular environment. As we previously

FIGURE 7 Lum Increases WT CFTR Protein Expression by a Proteostatic Mechanism and Restores Cerebral Perfusion in SAH

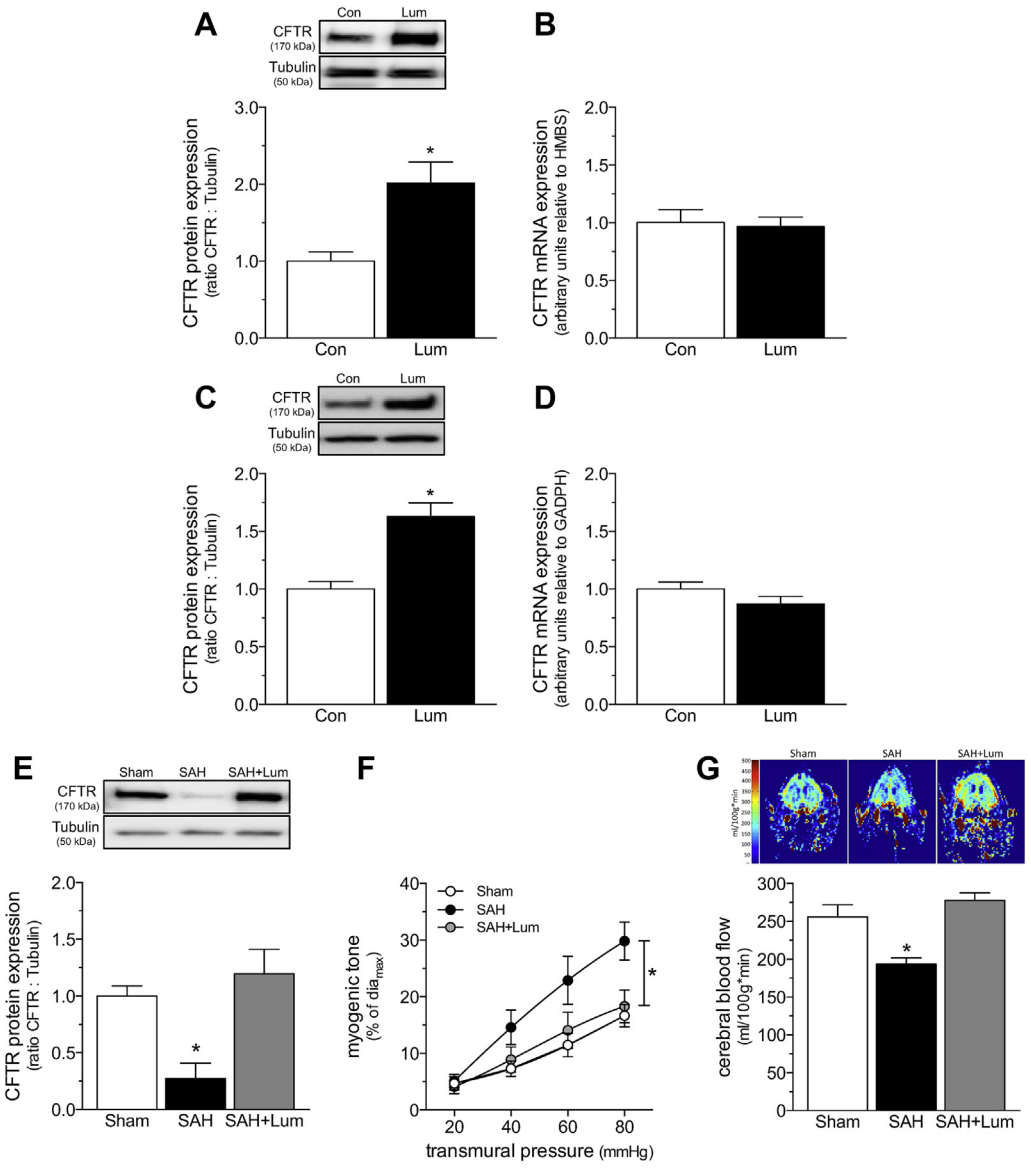

(A) Cerebral arteries isolated from naïve mice treated with Lum (3 mg/kg intraperitoneally daily for 2 days; n = 6) have higher CFTR protein expression than arteries collected from vehicle controls (n = 7). **(B)** Lum does not influence cerebral artery CFTR mRNA expression (n = 5 for both groups). **(C)** Lum (6 μmol/l; 24 h) increases CFTR protein expression in baby hamster kidney fibroblast cells stably expressing human CFTR (n = 13 for both groups). **(D)** Lum does not influence CFTR mRNA expression in this system (n = 6 for both groups). **(E)** Cerebral arteries isolated from mice with SAH (2 days post-SAH induction) have reduced CFTR protein expression (n = 5) relative to arteries isolated from sham-operated controls (n = 6). Lum treatment in vivo (3 mg/kg intraperitoneally daily for 2 days) eliminates this reduction in cerebral artery CFTR protein expression (n = 6). **(F)** Lum treatment in vivo reduces myogenic tone in olfactory arteries isolated from mice with SAH. Mean maximal vessel diameters at 45 mm Hg (dia_{max}) are sham: 91 ± 3 μm; n = 7 from 4 mice; SAH: 86 ± 2 μm; n = 6 from 3 mice; SAH+Lum: 87 ± 4 μm; n = 7 from 4 mice (1-way analysis of variance: p = NS). **(G)** Representative magnetic resonance perfusion maps that were used to determine CBF. SAH stimulated a reduction in cerebral perfusion; Lum treatment significantly improved cerebral perfusion in mice with SAH (sham: n = 6; SAH: n = 5; SAH+Lum: n = 6). All data are mean ± SEM. In **(A to D)**, * $p < 0.05$ for an unpaired comparison with a *t*-test; in **(E and G)**, *$p < 0.05$ for unpaired comparisons to sham with a 1-way analysis of variance test and Dunnett's post hoc test. In **(F)**, *$p < 0.05$ for unpaired comparisons to sham with a 2-way analysis of variance and Tukey's post hoc test. Abbreviations as Figures 1 to 3.

FIGURE 8 CFTR Correction Reduces Neuronal Injury in SAH

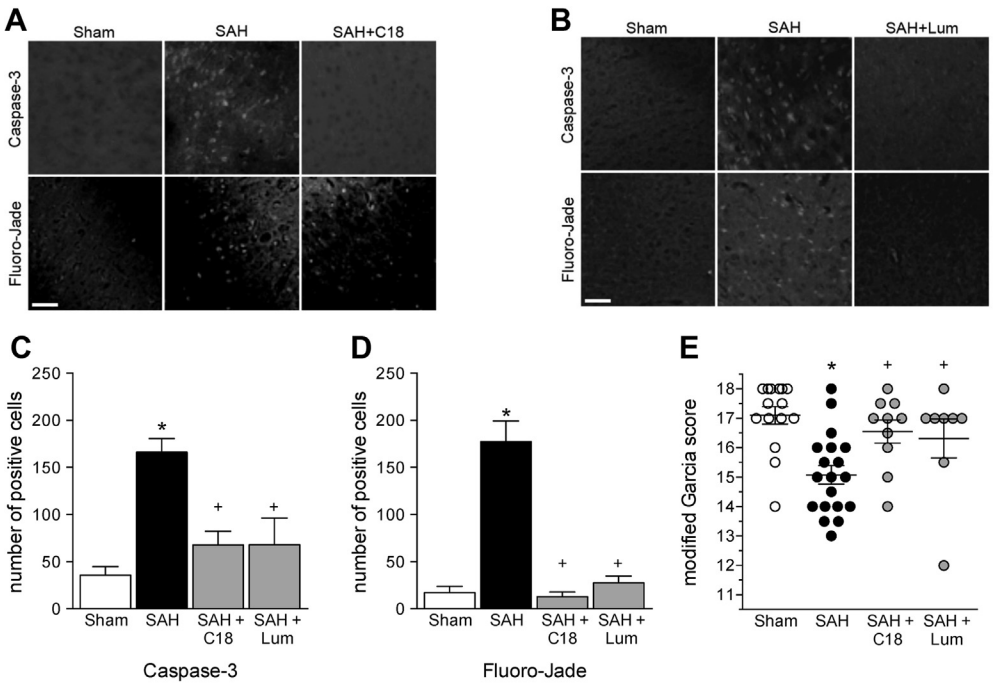

(Top) Representative images of cortical cells stained for cleaved caspase-3 expression and **(bottom)** with Fluoro-Jade for cohorts involving **(A)** C18 (3 mg/kg intraperitoneally daily for 2 days) and **(B)** lumacaftor (Lum) (3 mg/kg intraperitoneally daily for 2 days) treatment regimens. Subarachnoid hemorrhage (SAH) (n = 13 mice) increases the number of **(C)** caspase-3 and **(D)** Fluoro-Jade positive cells relative to sham-operated control mice (n = 12); both C18 (n = 6) and lumacaftor (n = 5) abolished the increase in caspase-3 and Fluoro-Jade staining. **(E)** Mice with SAH (n = 19) have a lower modified Garcia score (maximum score = 18; blinded assessments made 2 days post-SAH) compared with sham-operated mice (n = 15); both C18 (n = 10) and Lum (n = 8) treatment restored the neurological score to the sham level. All data are mean ± SEM; *p < 0.05 for unpaired comparisons to sham and +p < 0.05 compared with untreated SAH with a 1-way analysis of variance and Tukey's post hoc test.

demonstrated (8), TNF (10 ng/ml) reduced CFTR protein expression in primary vascular smooth muscle cells, and thus, simulated the TNF-dependent CFTR down-regulation observed in HF (8) and SAH (6) (**Figure 2E**). As expected, the decline in CFTR expression correlated with attenuated FITC-S1P uptake [i.e., a CFTR-dependent process (8)] (**Figure 2F**) and forskolin-stimulated iodide efflux [i.e., a classical measure of CFTR activity (16)] (**Figure 2G**). C18 treatment (6 μmol/l; 24 h co-incubation with 10 ng/ml TNF following 24-h incubation with 10 ng/ml TNF) reversed the decline in CFTR expression (**Figure 2E**) and fully restored FITC-S1P uptake (**Figure 2F**) and iodide efflux (**Figure 2G**). These results aligned with our prediction that under conditions in which CFTR is downregulated, C18's proteostatic effect increases total CFTR expression and restores its activity.

C18 TREATMENT RECTIFIES DEFICIENT CBF IN HF.

As previously documented by Meissner et al. (8), the induction of HF stimulated a significant reduction in cerebral artery CFTR protein expression (**Figure 3A**) that coincided with a marked augmentation in PCA myogenic tone (**Figure 3B**). As predicted by the data in **Figure 2**, C18 treatment in vivo (3 mg/kg intraperioneally daily for 2 days) restored CFTR expression in cerebral arteries isolated from mice with HF (**Figure 3A**) and concomitantly normalized PCA myogenic tone (**Figure 3B**). The attenuation of myogenic tone was associated with an expected shift in phenylephrine responsiveness, due to the reduction in basal tone; however, the EC_{50} values were not different (log EC_{50} sham: −6.30 ± 0.14; n = 6 from 4 mice; log EC_{50} HF: −6.25 ± 0.07; n = 5 from 3 mice; log EC_{50} HF+C18: −5.94 ± 0.21; n = 5 from 4 mice; 1-way analysis of variance: p = NS), and the curves overlapped after correction for the difference in basal tone (Supplemental Figure 4). C18 treatment did not affect PCA myogenic tone or phenylephrine responses in sham-operated mice (Supplemental Figure 5). Using PCAs isolated from CFTR knockout mice, we confirmed that C18 mediates its attenuating

effect on myogenic tone by targeting CFTR. As expected, PCAs from CFTR knockout mice displayed augmented myogenic tone that was not susceptible to in vivo C18 treatment (**Figure 3C**); phenylephrine responses were not affected by C18 treatment (Supplemental Figure 6).

At the systemic level, the induction of HF significantly reduced cardiac output relative to sham-operated control mice (**Figure 3D**; measured at 6 weeks post-infarction). TPR increased as a compensatory response (**Figure 3E**) to prevent a large reduction in MAP (**Figure 3F**) (4,8). Despite the relatively small reduction in MAP, CBF was markedly reduced (**Figure 3G**). C18 treatment in vivo restored CBF in mice with HF (**Figure 3G**), correlating to the normalization of PCA myogenic tone (**Figure 3B**). C18 did not ameliorate the cardiac injury induced by the left anterior descending coronary artery ligation procedure (Supplemental Table 2). Therefore, the improvement in CBF can be unambiguously attributed to a vascular mechanism. Furthermore, because C18 had no effect on TPR or MAP (**Figure 3**), the C18-mediated restoration of CBF had to be a localized microvascular effect that was independent of changes to systemic hemodynamic parameters. This therapeutic profile aligns well with our previously described etanercept intervention (4).

In addition to maintaining constant perfusion when systemic pressure fluctuates, the myogenic response also protects fragile capillary beds from damaging pressure levels (22) and maintains capillary hydrostatic pressure at levels that minimize edema formation (23). In this context, therapeutically reducing cerebral artery myogenic tone, even from the augmented level that occurs in HF, could potentially cause the counter-productive side effect of cerebral edema formation. Therefore, we used noninvasive imaging for edema to confirm that neither HF nor C18 treatment in the context of HF induced evident edema in any region of the brain (**Figure 4**).

C18 TREATMENT NORMALIZES HF-INDUCED CHANGES IN NEURONAL STRUCTURE AND MEMORY DEFICITS. Consistent with our previous histological analyses (5), HF significantly altered the morphology of pyramidal neurons in the frontal cortex. Specifically, HF (at 12 weeks post-infarction) induced 2 significant alterations: dendritic atrophy and a reduction in basal dendrite spine density (**Figure 5** and Supplemental Table 3). As shown in **Figure 5C** and summarized in Supplemental Table 3, HF did not affect the number of dendrite intersections. Because apical and basal dendrites can be differentially affected by stressors (24), we conducted a subanalysis to confirm that neither apical nor basal dendrite intersection morphology was affected (Supplemental Figure 7; Supplemental Table 3). However, our analysis demonstrated the presence of dendrite atrophy (i.e., a 22% reduction in dendrite length (**Figures 5C and 5D**) that was present in both apical (24% reduction) and basal (20% reduction) dendrites (Supplemental Figure 7). HF also reduced basal dendritic spine density in the distal regions of the dendrite (60 to 100 μm from the soma) (**Figure 5E and 5F**); apical dendritic spine density was not significantly altered (Supplemental Figure 8). C18-treated HF mice (3 mg/kg intraperioneally daily for 2 weeks) did not display dendrite atrophy or a reduction in dendritic spine density (**Figure 5**, Supplemental Figure 8, Supplemental Table 3).

The altered cortical neuron morphology in HF mice correlated with impaired rhino-cortical–dependent, short-term retention of object familiarity (**Figure 5G**); this impairment was not present in C18-treated HF mice. Longitudinal pre-treatment (i.e., at 10 weeks post-infarction) and post-treatment analyses of the same vehicle- and C18- treated HF mice confirmed that C18 reversed the impairment caused by HF (**Figure 5H**).

Importantly, the C18-mediated normalization of histological and cognitive parameters is not attributable to improved cardiac function because the ejection fraction did not change following C18 treatment (3 mg/kg intraperioneally daily for 2 weeks; pre-C18 ejection fraction: 47 ± 3%; post-C18 ejection fraction: 46 ± 3%; n = 8; paired *t* test: p = NS). We also confirmed that the vehicle- and C18-treated groups possessed comparable reductions in ejection fraction at the 2 weeks post-treatment time point (sham: 64 ± 2%, n = 8; HF: 46 ± 4% *; n = 7; HF+C18: 46 ± 3% *; n = 8; * denotes $p < 0.05$ for both HF and HF+C18 relative to sham; p = NS for HF relative to HF+C18 following unpaired comparisons with a 1-way analysis of variance and Tukey's post hoc test).

C18 TREATMENT RECTIFIES DEFICIENT CBF IN SAH. Our previous work demonstrated that SAH has a similar cerebrovascular phenotype as HF, in that 1) cerebral artery CFTR protein expression is reduced; 2) cerebral artery myogenic tone is augmented; and 3) cerebral perfusion is reduced (6). As in HF (**Figure 3**), C18 treatment in vivo (3 mg/kg intraperioneally daily for 2 days) restored CFTR expression in cerebral arteries from mice with SAH (**Figure 6A**) and

concomitantly normalized olfactory cerebral artery myogenic tone (**Figure 6B**). The attenuation of myogenic tone was associated with an expected baseline shift in phenylephrine responsiveness, due to the reduction in basal tone; however, the EC_{50} values were not different (log EC_{50} sham: -5.52 ± 0.23; $n = 5$ from 3 mice; log EC_{50} SAH: -6.01 ± 0.16; $n = 6$ from 6 mice; log EC_{50} SAH+C18: -6.01 ± 0.31; $n = 5$ from 4 mice; 1-way analysis of variance: $p = NS$), and the curves overlapped after correction for the difference in basal tone (Supplemental Figure 9). C18 treatment did not affect olfactory cerebral myogenic tone or phenylephrine responses in sham-operated mice (Supplemental Figure 10). Using olfactory cerebral arteries isolated from CFTR knockout mice, we confirmed that C18 mediated its attenuating effect on myogenic tone by targeting CFTR. As expected, olfactory cerebral arteries from CFTR knockout mice displayed augmented myogenic tone that was not susceptible to in vivo C18 treatment (**Figure 6C**); phenylephrine responsiveness in these arteries was not affected by C18 treatment (Supplemental Figure 11). Importantly, in vivo C18 treatment restored CBF (**Figure 6D**), once again correlating with the normalization of olfactory cerebral artery myogenic tone (**Figure 6B**).

LUMACAFTOR TREATMENT RECTIFIES DEFICIENT CBF IN SAH. We complemented our C18 data with interventions that used the CFTR corrector lumacaftor, a clinically relevant C18 analogue that is approved by the Food and Drug Administration for treating cystic fibrosis, in combination with the CFTR potentiator ivacaftor (i.e., Orkambi; Vertex, Boston, Massachusetts). We first confirmed that lumacaftor was capable of increasing both mouse and human CFTR expression. As observed for C18 (**Figure 2**), lumacaftor increased CFTR protein expression in mouse cerebral arteries (mice injected with 3 mg/kg intraperitoneally daily for 2 days) and baby hamster kidney fibroblast cells that stably expressed human CFTR (**Figure 7**). In both settings, CFTR mRNA expression was unaffected, indicating a nontranscriptional mechanism (**Figure 7**). Consistent with our C18 data in SAH (**Figure 6**), lumacaftor treatment in vivo (3 mg/kg intraperitoneally daily for 2 days) restored CFTR expression in cerebral arteries from SAH mice (**Figure 7**) and concomitantly normalized olfactory cerebral artery myogenic tone and cerebral perfusion (**Figure 7**). Lumacaftor did not affect phenylephrine responsiveness (Supplemental Figure 12) and consequently, the EC_{50} values were not different (log EC_{50} sham: -5.79 ± 0.09; $n = 7$ from 4 mice; log EC_{50} SAH: -5.93 ± 0.19; $n = 6$ from 3 mice; log EC_{50} SAH+Lum: -5.90 ± 0.18; $n = 7$ from 4 mice; 1-way analysis of variance: $p = NS$).

C18 AND LUMACAFTOR REDUCE NEURONAL INJURY IN SAH. The neuronal injury induced by SAH can be easily characterized with standard histological techniques (Fluoro-Jade and activated caspase-3 staining) and simple neurologic testing (Modified Garcia Score) (6); we used these methods to determine whether the restoration of normal myogenic responsiveness and CBF correlated with improved neurologic function in the delayed ischemia phase of the SAH disease. Both C18 and lumacaftor significantly attenuated neuronal injury at 2 days post-SAH, as assessed by activated caspase-3 and Fluoro-Jade staining (**Figure 8**); these neuronal injury reductions correlated with improved neurologic function (**Figure 8E**). Specifically, SAH mice scored lower than sham-operated mice on the modified Garcia neurologic function test. However, C18- and lumacaftor-treated SAH mice had neurologic function scores comparable to sham-operated mice.

DISCUSSION

This investigation demonstrated that CFTR is a prominent regulator of cerebral perfusion, and consequently, is a therapeutic target. In experimental models of HF and SAH, cerebral artery CFTR expression was downregulated; the loss of CFTR activity augmented myogenic vasoconstriction, thereby increasing vascular resistance, and consequently, reducing cerebral perfusion. Therapeutic agents that restored CFTR expression in these pathological settings normalized cerebrovascular reactivity and perfusion. These improvements correlated with improved neurologic injury and function. Therefore, CFTR therapeutics may represent an untapped resource for clinically managing injurious cerebral perfusion deficits, and hence, neurologic outcome in patients with HF and SAH.

The CFTR corrector compounds C18 and lumacaftor were originally developed to chaperone misfolded mutant CFTR proteins to the plasma membrane. This indication does not apply to patients with HF and SAH, because 1) most patients possess wild-type CFTR; and 2) the pathological reduction in CFTR activity is due to a transcription-based mechanism, not a trafficking defect. Thus, it was necessary to confirm that C18 and lumacaftor increased wild-type CFTR abundance. Our data showed that C18 and lumacaftor increased wild-type CFTR abundance by a nontranscriptional, proteostatic mechanism.

This is consistent with a separate study that demonstrated the stabilization of cell surface–localized CFTR against internalization and subsequent degradation (21). Over time, stabilizing cell surface CFTR elevates overall CFTR expression levels because less cell surface CFTR was internalized and routed to degradation mechanisms.

We strategically selected proximal PCAs for our HF studies and olfactory cerebral arteries for our SAH studies to directly compare the CFTR-targeted interventions to our previous work (4,6,8). Although PCAs and olfactory arteries originate from distinct regions of the cerebral microcirculation (i.e., posterior and anterior, respectively) and display differences in their baseline myogenic tone curves, they behave similarly in terms of the pathological signaling mechanisms that augment myogenic responsiveness (4,6,8). The comparable success of the CFTR-targeted interventions in PCAs and olfactory arteries suggests that CFTR regulates vascular reactivity broadly throughout the cerebral microcirculation.

To increase brain perfusion, cerebrovascular resistance must decrease in relation to TPR. We therefore compared the role that CFTR plays in cerebral arteries to skeletal muscle resistance arteries. We selected skeletal muscle resistance arteries for this comparison, because this vascular bed forms the body's largest circulatory network (40% of body mass is skeletal muscle); therefore, it is a prominent determinant of TPR. Our comparisons of 1) CFTR inhibition in cerebral and skeletal muscle resistance arteries, and 2) TPR measurements in CFTR mutant and wild-type mice indicated that CFTR's vascular effects do not appreciably influence MAP. This is presumably explained by the observed differences in CFTR expression across these vascular beds: skeletal muscle resistance arteries have 10-fold lower CFTR expression than do cerebral arteries. Therefore, CFTR therapeutics should exhibit similarly restricted effects. CFTR corrector treatment increases cerebral perfusion without affecting TPR. This specific effect is highly advantageous because the lack of a direct effect on peripheral resistance increases the likelihood that the intervention can be added to prescribed blood pressure management practices that would already be in place.

The myogenic response, which continuously matches vascular resistance to the prevalent transmural pressure (25,26), is the functional basis of CBF autoregulation. In addition to dictating cerebral perfusion through its autoregulatory function, the myogenic response also maintains capillary pressures at levels that minimize damage and edema formation (22,23). Therefore, reducing myogenic reactivity has the potential to induce edema formation by permitting additional pressure to enter the capillary beds. On a related aspect, because S1P prominently regulates blood–brain barrier permeability (27), CFTR-dependent changes in S1P signaling could cause edema through alterations in barrier function. Thus, it was crucial to exclude edema as a negative effect of our intervention. CFTR corrector treatment (C18) did not induce edema in mice with HF. This confirmed that: 1) hydrostatic pressure in the cerebral microcirculation remained within tolerable limits (this would be expected because the CBF and MAP measures were comparable to sham animals); and 2) blood–brain barrier function was preserved during treatment.

A key translational question is whether CFTR regulates vasoconstriction in the human cerebrovascular microcirculation. To our knowledge, cerebrovascular CFTR expression has never been assessed in human cerebral arteries, nor has cerebral perfusion been systematically assessed in patients with cystic fibrosis. Our previous translational work that compared human and/or mouse mesenteric and skeletal muscle artery CFTR expression and function (28) provides a decent hint. As observed in the mouse, human mesenteric arteries both express CFTR and display functional sensitivity to CFTR inhibition, whereas human skeletal muscle resistance arteries possess no detectable CFTR protein and are consequently insensitive to CFTR inhibition (28). Thus, the functional profile for mesenteric and skeletal muscle resistance arteries overlapped in mice and humans, providing reasonable grounds to speculate that CFTR's functional role in the mouse cerebral microcirculation will also translate to the human setting.

We previously showed that HF downregulates CFTR expression in lung terminal bronchiolar epithelial cells (8), and thus, reductions in CFTR expression were not restricted to the vascular system. It is therefore tempting to speculate that CFTR therapeutics could provide other substantive benefits beyond the improvement of cerebral perfusion. In contrast, it is not known whether the HF and SAH pathologies ubiquitously downregulate CFTR expression in all tissues, meaning that CFTR therapeutics could also have unanticipated, nonbeneficial effects in other tissues by increasing CFTR expression above normal levels. At present, clinical trial data for lumacaftor and lumacaftor/ivacaftor in healthy subjects are proprietary, and therefore, are not publicly available. However, NIH clinical trial records indicate that several safety studies in healthy subjects have

been completed and more are ongoing. The consecutive initiation of clinical trials in healthy patients is a strong, yet indirect indication that no serious adverse events have been encountered to date. As a Food and Drug Administration–approved medication in combination with ivacaftor, lumacaftor has already cleared rigorous standards for safety and toxicity (13,29).

HF and SAH are fundamentally different pathologies that share a common aspect of downregulated cerebral artery CFTR expression (6,8). One key strength of the present investigation was that we demonstrated therapeutic efficacy in 2 distinct injury processes with markedly different severities. The "delayed cerebral ischemia" that occurrs at 2 days post-SAH causes acute, irrevocable neuronal injury. Thus, we targeted CFTR as a preventative intervention against a severe insult. The cerebral effects of HF were not nearly as overt, largely because the primary injury occurred at the heart rather than in the brain. Chronic malperfusion induced reversible neurologic deficits via dendritic atrophy and reduced synaptic strength [i.e., reduced spine density (30)]. In this context, we delayed treatment in HF until cognitive impairment was evident and then targeted CFTR as a means of restoring normal neuronal function. Therefore, our investigation demonstrated that therapeutically targeting CFTR can 1) improve outcomes in multiple, etiologically distinct pathologies; 2) prevent acute, irreversible neuronal injury; and 3) reverse deleterious alterations in neuronal connectivity. In addition to establishing the broad usefulness of targeting CFTR as an intervention, the fact that therapeutic success was observed across the 2 etiologically distinct disease models argues against a nonspecific or off-target effect of the intervention.

As a caveat, the SAH vasculopathy is not solely defined by a functional abnormality in myogenic reactivity and autoregulation. As demonstrated by Sabri et al. (31), an SAH model similar to ours elicited marked morphological changes to microvascular structure, including increased wall thickness and a convoluted and/or irregular luminal surface. Although Sabri et al. also demonstrated reduced luminal diameter in microvessels, the relative contributions of aberrant vasoconstriction (e.g., augmented myogenic tone) and structural changes to this deficit could not be discerned (31). In the present investigation, SAH had no effect on maximal luminal diameter, which was determined under calcium-free conditions to yield maximal dilation. Thus, we have no evidence that structural changes contributed to the perfusion deficits we observed. Nevertheless, pathological changes to cerebrovascular structure have the potential to significantly alter vascular reactivity and cerebral perfusion and warrant further investigation.

CONCLUSIONS

The present investigation provides direct evidence that CFTR regulates cerebrovascular reactivity and validates CFTR as a therapeutic target for normalizing cerebral perfusion deficits in HF and SAH. Both HF and SAH reduced cerebral perfusion by downregulating cerebral artery CFTR protein expression, thereby compromising autoregulatory control. This study demonstrated that clinically available CFTR therapeutics can restore cerebral artery CFTR expression, vascular reactivity, and cerebral perfusion. Remarkably, this therapeutic effect appears to be primarily localized to the cerebral microcirculation because CFTR does not modulate the reactivity of peripheral arteries involved in blood pressure control. Therefore, CFTR therapeutics could emerge as valuable clinical tools to manage cerebrovascular dysfunction, impaired cerebral perfusion, and neuronal injury. The observations presented herein encourage an immediate clinical assessment of CFTR therapeutics for the prevention and improvement of cerebral perfusion deficits in HF and SAH.

ACKNOWLEDGMENTS The authors gratefully acknowledge the Lund University Bioimaging Center for providing access to the Nikon Eclipse T*i*2 microscope system.

ADDRESS FOR CORRESPONDENCE: Dr. Steffen-Sebastian Bolz, Toronto Centre for Microvascular Medicine at TBEP, University of Toronto, 661 University Avenue, 14th Floor, Toronto, Ontario, Canada, M5G 1M1. E-mail: sts.bolz@utoronto.ca.

PERSPECTIVES

COMPETENCY IN MEDICAL KNOWLEDGE: Both HF and SAH reduce cerebral perfusion by altering autoregulatory control mechanisms. Because current medical interventions do not target these causal mechanisms, they display limited efficacy. Restoring normal myogenic reactivity in cerebral arteries represents a significant advantage over current strategies.

TRANSLATIONAL OUTLOOK: These data provide strong proof of principle for clinically assessing whether CFTR therapeutics improve cerebral perfusion in patients with HF and SAH.

REFERENCES

1. Román GC. Brain hypoperfusion: a critical factor in vascular dementia. Neurol Res 2004;26:454–8.

2. Doehner W, Ural D, Haeusler KG, et al. Heart and brain interaction in patients with heart failure: overview and proposal for a taxonomy. A position paper from the Study Group on Heart and Brain Interaction of the Heart Failure Association. Eur J Heart Fail 2018;20:199–215.

3. Wong GK, Lam S, Ngai K, et al. Evaluation of cognitive impairment by the Montreal cognitive assessment in patients with aneurysmal subarachnoid haemorrhage: prevalence, risk factors and correlations with 3 month outcomes. J Neurol Neurosurg Psychiatry 2012;83:1112–7.

4. Yang J, Hossein Noyan-Ashraf M, Meissner A, et al. Proximal cerebral arteries develop myogenic responsiveness in heart failure via tumor necrosis factor-α-dependent activation of sphingosine-1-phosphate signaling. Circulation 2012;126:196–206.

5. Meissner A, Visanji NP, Momen MA, et al. Tumor necrosis factor-α underlies loss of cortical dendritic spine density in a mouse model of congestive heart failure. J Am Heart Assoc 2015;4:e001920.

6. Yagi K, Lidington D, Wan H, et al. Therapeutically targeting tumor necrosis factor-α/sphingosine-1-phosphate signaling corrects myogenic reactivity in subarachnoid hemorrhage. Stroke 2015;46:2260–70.

7. Xiao M, Li Q, Feng H, Zhang L, Chen Y. Neural vascular mechanism for the cerebral blood flow autoregulation after hemorrhagic stroke. Neural Plast 2017;2017:5819514.

8. Meissner A, Yang J, Kroetsch JT, et al. Tumor necrosis factor-α-mediated downregulation of the cystic fibrosis transmembrane conductance regulator drives pathological sphingosine-1-phosphate signaling in a mouse model of heart failure. Circulation 2012;125:2739–50.

9. Nakamura H, Yoshimura K, Bajocchi G, Trapnell BC, Pavirani A, Crystal RG. Tumor necrosis factor modulation of expression of the cystic fibrosis transmembrane conductance regulator gene. FEBS Lett 1992;314:366–70.

10. Besançon F, Przewlocki G, Baró I, Hongre AS, Escande D, Edelman A. Interferon-gamma downregulates CFTR gene expression in epithelial cells. Am J Physiol 1994;267:C1398–404.

11. Murdaca G, Spanò F, Contatore M, et al. Infection risk associated with anti-TNF-α agents: a review. Expert Opin Drug Saf 2015;14:571–82.

12. Kroetsch JT, Levy AS, Zhang H, et al. Constitutive smooth muscle tumour necrosis factor regulates microvascular myogenic responsiveness and systemic blood pressure. Nat Commun 2017;8:14805.

13. Boyle MP, Bell SC, Konstan MW, et al. A CFTR corrector (lumacaftor) and a CFTR potentiator (ivacaftor) for treatment of patients with cystic fibrosis who have a phe508del CFTR mutation: a phase 2 randomised controlled trial. Lancet Respir Med 2014;2:527–38.

14. van Doorninck JH, French PJ, Verbeek E, et al. A mouse model for the cystic fibrosis delta F508 mutation. EMBO J 1995;14:4403–11.

15. Loubinoux I, Volk A, Borredon J, et al. Spreading of vasogenic edema and cytotoxic edema assessed by quantitative diffusion and T2 magnetic resonance imaging. Stroke 1997;28:419–26.

16. Malik FA, Meissner A, Semenkov I, et al. Sphingosine-1-phosphate is a novel regulator of cystic fibrosis transmembrane conductance regulator (CFTR) activity. PLoS One 2015;10:e0130313.

17. Lueptow LM. Novel object recognition test for the investigation of learning and memory in mice. J Vis Exp 2017;126:e55718.

18. Wilke M, Buijs-Offerman RM, Aarbiou J, et al. Mouse models of cystic fibrosis: phenotypic analysis and research applications. J Cyst Fibros 2011;10 Suppl 2:S152–71.

19. Lavelle GM, White MM, Browne N, McElvaney NG, Reeves EP. Animal models of cystic fibrosis pathology: phenotypic parallels and divergences. Biomed Res Int 2016;2016:5258727.

20. Korthuis RJ. Regulation of vascular tone in skeletal muscle. In: Granger DN, Granger J, editors. Skeletal Muscle Circulation. San Rafael, CA: Morgan & Claypool Life Sciences, 2011:7–34.

21. Okiyoneda T, Veit G, Dekkers JF, et al. Mechanism-based corrector combination restores ΔF508-CFTR folding and function. Nat Chem Biol 2013;9:444–54.

22. Bidani AK, Griffin KA, Williamson G, Wang X, Loutzenhiser R. Protective importance of the myogenic response in the renal circulation. Hypertension 2009;54:393–8.

23. Moien-Afshari F, Skarsgard PL, McManus BM, Laher I. Cardiac transplantation and resistance artery myogenic tone. Can J Physiol Pharmacol 2004;82:840–8.

24. Cook SC, Wellman CL. Chronic stress alters dendritic morphology in rat medial prefrontal cortex. J Neurobiol 2004;60:236–48.

25. Paulson OB, Strandgaard S, Edvinsson L. Cerebral autoregulation. Cerebrovasc Brain Metab Rev 1990;2:161–92.

26. Toth P, Tarantini S, Csiszar A, Ungvari Z. Functional vascular contributions to cognitive impairment and dementia: mechanisms and consequences of cerebral autoregulatory dysfunction, endothelial impairment, and neurovascular uncoupling in aging. Am J Physiol Heart Circ Physiol 2017;312:H1–20.

27. Prager B, Spampinato SF, Ransohoff RM. Sphingosine 1-phosphate signaling at the blood-brain barrier. Trends Mol Med 2015;21:354–63.

28. Hui S, Levy AS, Slack DL, et al. Sphingosine-1-phosphate signaling regulates myogenic responsiveness in human resistance arteries. PLoS One 2015;10:e0138142.

29. Wainwright CE, Elborn JS, Ramsey BW, et al. Lumacaftor-ivacaftor in patients with cystic fibrosis homozygous for Phe508del CFTR. N Engl J Med 2015;373:220–31.

30. Nimchinsky EA, Sabatini BL, Svoboda K. Structure and function of dendritic spines. Annu Rev Physiol 2002;64:313–53.

31. Sabri M, Ai J, Lakovic K, D'abbondanza J, Ilodigwe D, Macdonald RL. Mechanisms of microthrombi formation after experimental subarachnoid hemorrhage. Neuroscience 2012;224:26–37.

KEY WORDS cognitive impairment, corrector compounds, cystic fibrosis transmembrane conductance regulator (CFTR), myogenic vasoconstriction, sphingosine-1-phosphate, tumor necrosis factor, vascular smooth muscle cells

APPENDIX For an expanded Methods section and supplemental figures and tables, please see the online version of this paper.